

# High-performance aqueous asymmetric electrochemical capacitors based on graphene oxide/cobalt(II)-tetrapyrazinoporphyrazine hybrid†

Cite this: *J. Mater. Chem. A*, 2013, **1**, 2821

Joel N. Lekitima,<sup>a</sup> Kenneth I. Ozoemena,<sup>\*ab</sup> Charl J. Jafta,<sup>bc</sup> Nagao Kobayashi,<sup>\*d</sup> Yang Song,<sup>e</sup> Dennis Tong,<sup>e</sup> Shaowei Chen<sup>\*e</sup> and Munetaka Oyama<sup>f</sup>

A novel asymmetric electrochemical capacitor (AEC) with high energy and power densities has been developed using a graphene oxide/cobalt(II)tetrapyrazinoporphyrazine composite (GO/CoTPyzPz) as the positive electrode and graphene oxide/carbon black (GO/CB) as the negative electrode in a neutral aqueous Na<sub>2</sub>SO<sub>4</sub> electrolyte. The excellent specific capacitance, energy and power densities (~500 F g<sup>-1</sup>, 44 W h kg<sup>-1</sup> and 31 kW kg<sup>-1</sup>) coupled with long cycle life, excellent short response time, and low equivalent series resistance clearly indicate that this new material has great potential for the development of low-cost and 'green' aqueous AECs that operate at high energy and power densities. Interestingly, the energy density of the GO/CoTPyzPz//GOCB based AEC falls within the range usually observed for nickel metal hydride (NiMH) batteries (30–100 W h kg<sup>-1</sup>), but more importantly, shows better power performance than NiMH batteries (0.25–1 kW kg<sup>-1</sup>) widely used in hybrid vehicles such as Toyota Prius and Honda Insight.

Received 1st December 2012

Accepted 19th December 2012

DOI: 10.1039/c2ta01325h

www.rsc.org/MaterialsA

## 1 Introduction

Metallo-tetrapyrazinoporphyrazines (MTPyzPz, Fig. 1) are aza-analogues of the well-known metallophthalocyanine (MPC) macrocycles, which have been known since the early 1960s,<sup>1</sup> and have recently attracted interest in photochemistry.<sup>2–4</sup> Since the first report of their electrochemical behaviour towards oxygen reduction reaction by Kobayashi *et al.*<sup>5</sup> two decades ago, there has been no study on any other possible electrochemical applications. Unlike their MPC counterparts,<sup>6–8</sup> there is no report on the electrochemical capacitive properties of MTPyzPz. This is one of the primary motivations for the present study.

Electrochemical capacitors (ECs) are energy storage devices with high power density, long lifetime and large cycling capability. They bridge the power–energy gap between traditional dielectric capacitors (high power) and batteries (high energy).

They are useful in a plethora of energy capture and storage applications, either by themselves as the primary power source or in combination with batteries or fuel cells.

Asymmetric ECs, also known as hybrid supercapacitors, which are characterised by Faradaic reactions (pseudo-capacitance) and charge-storage (electric double layer capacitance), have begun to receive immense research interest because of their high energy density, large power density and long lifetime.<sup>9</sup>

Graphene oxide (GO) is a single sheet of graphite oxide, and an intermediate product during graphene synthesis by the well-known method of oxidation–exfoliation–reduction of graphite

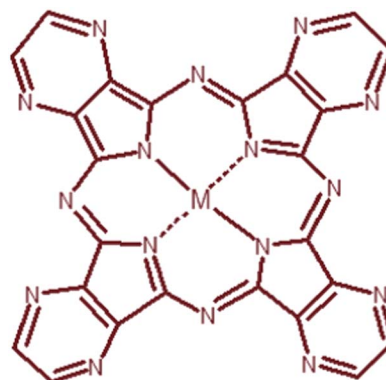


Fig. 1 Molecular structure of metallo-tetrapyrazinoporphyrazines (MTPyzPz, where M = metal, and in this work, Co).

<sup>a</sup>Department of Chemistry, University of Pretoria, Pretoria 0002, South Africa

<sup>b</sup>Energy Materials, Materials Science and Manufacturing, Council for Scientific & Industrial Research (CSIR), Pretoria 0001, South Africa. E-mail: kozoemena@csir.co.za; Fax: +27 12 841 2135; Tel: +27 12 841 3664

<sup>c</sup>Department of Physics, University of Pretoria, Pretoria 0002, South Africa

<sup>d</sup>Department of Chemistry, Graduate School of Science, Tohoku University, Sendai, 980-8578, Japan. E-mail: nagaok@m.tohoku.ac.jp

<sup>e</sup>Department of Chemistry and Biochemistry, University of California, Santa Cruz, California, USA. E-mail: shaowei@ucsc.edu

<sup>f</sup>Department of Material Chemistry, Graduate School of Engineering, Kyoto University, Nishikyo-ku, Kyoto 615-8520, Japan

† Electronic supplementary information (ESI) available: AFM, Raman spectroscopy, and FTIR. See DOI: 10.1039/c2ta01325h

powder. Although it is theoretically claimed not to be suitable for supercapacitor application,<sup>10</sup> Xu *et al.*<sup>11</sup> have recently shown that they exhibit higher capacitance than graphene due to the extra pseudo-capacitance effect of the attached oxygen-containing functional groups on its basal planes. Given its higher capacitance, lower cost and shorter processing time than reduced graphene oxide (RGO), GO has been described as a better choice than RGO for supercapacitors.

Our interest in the GO/MTPyzPz hybrid for AEC stems from two possibilities. First, the  $\pi$ -delocalization on the MTPyzPz allows for strong  $\pi$ - $\pi$  interactions with the GO. Second, it is well established that surface functional groups containing oxygen<sup>12-14</sup> and nitrogen<sup>15,16</sup> significantly improve the total capacitance through the extra pseudo-capacitance effects, as well as enhanced wettability of porous carbon with electrolytes. Thus, the high nitrogen content of the MTPyzPz and the oxygen content of the GO will offer a good synergy for enhanced capacitance.

This paper describes the properties of a GO/CoTPyzPz hybrid as a high-energy, high-power asymmetric electrochemical capacitor in neutral aqueous solutions. As elegantly articulated by Long *et al.*,<sup>17</sup> aqueous asymmetric ECs offer various attractive features, notably (i) simplified fabrication and packaging procedures that avoid rigorous environmental controls; (ii) a higher degree of safety compared to the use of organic-based ECs with respect to thermal stability and runaway; (iii) the use of less toxic and lower cost electrolytes; and (iv) specific energy that meets or exceeds those of nonaqueous EDLCs. In this work, the GO/CoTPyzPz based aqueous EC exhibits an extraordinarily high specific energy (44 W h kg<sup>-1</sup>, comparable with NiMH batteries, 30–100 W h kg<sup>-1</sup>), exceptional power density (31 kW kg<sup>-1</sup>, comparable to conventional capacitors and higher than NiMH batteries, 0.25–1 kW kg<sup>-1</sup>, that are now widely used in hybrid vehicles such as Toyota Prius and Honda Insight<sup>18</sup>) and an exceptional specific capacitance of 500 F g<sup>-1</sup>. In addition, the electrode shows excellent stability of over 300 charge–discharge continuous cycles. Electrochemical impedance study proves that most of the stored energy can be accessible at high frequencies (63 Hz).

## 2 Experimental

The CoTPyzPz compounds were synthesized and characterised as reported by Kobayashi *et al.*<sup>5</sup> The GO was prepared using the modified Hummers' method from graphite powders.<sup>19</sup> In brief, 0.5 g of graphite powders and 0.5 g of NaNO<sub>3</sub> were mixed with 23 mL of concentrated H<sub>2</sub>SO<sub>4</sub> under magnetic stirring for 10 min in a clean flask at 0 °C. 3 g of KMnO<sub>4</sub> was then slowly added into the above solution in 3 min to prevent a sudden temperature increase. Then the dark greenish solution was transferred to a 35 ± 5 °C water bath and stirred for about 1 h. Next, 50 mL of water was added slowly, and the solution was stirred for another 30 min while the temperature was raised to 90 ± 5 °C. After adding 150 mL of water, 3 mL of H<sub>2</sub>O<sub>2</sub> (30%) was added drop-wise, resulting in the formation of a brownish solution. Finally, the warm solution was filtered and washed with 50 mL of hydrochloric acid solution (0.1 M) and 500 mL of water,

respectively. The filter cake was then dispersed in water by sonication using a table-top ultrasonic cleaner (VWR B1500-A MTH, 50W). The products were then separated *via* centrifugation for 5 min to remove all visible particles. The last sediment was redispersed in water under mild sonication, which resulted in a homogeneous brown solution of exfoliated GO. The GO/CoTPyzPz hybrid was obtained by milling an equal amount of CoTPyzPz and GO (1 : 1 mass ratio), dissolved in DMF, ultrasonicated for 30 min and finally dried.

Electrochemical measurements were performed in a single-cell configuration using coin cells (LIR-2032). A 1 M Na<sub>2</sub>SO<sub>4</sub> solution served as the electrolyte while a glass microfiber served as the separator. Prior to use, the nickel foam (current collector) was cleaned in a 1 M HCl solution, washed with a copious amount of de-ionized water, and dried under vacuum. The positive electrode (GO/CoTPyzPz hybrid) was prepared by mixing CoTPyzPz, GO, carbon black (CB) and polyvinylidene fluoride (PVDF) in a mass ratio of 4 : 4 : 1 : 1 using pestle and mortar and dispersing in a few drops of anhydrous *N*-methyl-2-pyrrolidone to produce a homogeneous paste. The CB and PVDF served as the conductive agent and binder, respectively. The resulting slurry was coated onto the nickel foam substrate (201 cm<sup>2</sup>) with a spatula. The electrode was then dried at 80 °C for 8 h in a vacuum oven, and pressed to a thickness of ~0.5 mm. The negative electrode was prepared using the same procedure but with CB, GO and PVDF in a mass ratio of 8 : 1 : 1. The mass loading ratio (positive electrode/negative electrode) is 0.4. The cell was tested after 24 h of fabrication. For comparison, symmetric cells of GO and CoTPyzPz were prepared.

GO samples were prepared for high resolution transmission electron microscopy (HR-TEM) by drop-casting a dilute (1 mg mL<sup>-1</sup>) aqueous solution of graphene oxide onto a lacey carbon coated 400 mesh copper grids. The electron microscope was a modified Philips CM300FEG/UT operating at 300 kV. Raman spectroscopy data were collected on a Jobin Yvon Horiba TX 6400 micro-Raman spectrometer equipped with a triple monochromator system to eliminate contributions from the Rayleigh line and LabSpec (Ver. 5.78.24) analytical software. Samples were analysed with a 514 nm Argon excitation laser (1.5 mW laser power on the sample to avoid thermal effects), a 50× objective with recording times ranging between 120 s. All AFM images were obtained under ambient conditions with an Agilent 5500 microscope (Agilent Technologies, USA) in acoustic mode (tapping mode) at a scanning frequency of 1 Hz. Silicon cantilevers with a nominal resonant frequency and force constant of ~330 kHz and 40 N m<sup>-1</sup>, respectively, were used for imaging. Cyclic voltammetry, galvanostatic charge–discharge measurements, and electrochemical impedance spectroscopy (EIS) were carried out using an Autolab potentiostat PGSTAT 302N (Eco Chemie, Utrecht, The Netherlands) driven by the General Purpose Electrochemical Systems data processing software (GPES and FRA software version 4.9). Cyclic voltammetry was done in a three-electrode system with the active material coated on Ni foam as the working electrode, Pt as the counter electrode and Ag/AgCl as the reference electrode. EIS data were obtained with the Autolab Frequency Response Analyser (FRA) software between 100 kHz and

10 mHz with a perturbation amplitude (rms value) of the ac signal of 3 mV. Every EIS experiment was performed after allowing the electrode to equilibrate for 5 min at the chosen fixed potential.

### 3 Results and discussion

#### Microscopic and spectroscopic characterization

A graphene oxide sheet obtained by the modified Hummers' method<sup>19</sup> is shown in Fig. 2. The smooth sheet may be identified in the micrograph, while the edges tend to fold and roll. Lattice fringes are visible on the edges of graphene oxide sheets due to folds and/or rolls, as can be seen in the HRTEM image in Fig. 2. The separation between neighbouring fringes (Fig. 2, inset) was measured to be  $\sim 0.37$  nm and is larger than the interplanar spacing in graphite (0.335 nm),<sup>20</sup> which can be attributed to the presence of oxygen functional groups on the graphene oxide layers.

From the FESEM images of the GO, CoTPyzPz and GO/CoTPyzPz hybrid (Fig. 3), both the CoTPyzPz and GO/CoTPyzPz sizes ranged from nano-sized to sub-micron-sized crystalline structures.

Fig. 4 shows the UV/Vis spectra of GO, CoTPyzPz, and GO-CoTPyzPz in DMF. The GO spectrum presented an adsorption peak around 260 nm ( $\pi-\pi^*$  transition). CoTPyzPz showed the characteristic Q band at 630 nm with a shoulder at 730 nm (due to aggregation<sup>4</sup>), a vibrational  $Q_{0-0}$  band at 577 nm, a weak band around 430 nm due to metal-ligand charge-transfer (MLCT) transition, and a B band at 345 nm. Upon integration with the GO, the original Q-band of CoTPyzPz at 630 nm almost disappeared, slightly blue-shifted to 621 nm, while the peak at 730 nm became broader and more pronounced. This incredible change in the UV-Vis spectrum is a clear indication of the interaction between the GO and CoTPyzPz *via* strong cofacial aggregation (face-to-face assembly). The slight blue shift suggests that the energy gap between the HOMO and LUMO of the GO-CoTPyzPz hybrid has become wider than that of CoTPyzPz.<sup>21,22</sup> The cofacial aggregation should result in maximum contact between the CoTPyzPz molecules and the graphene sheet, thus leading to a fast electron transport through the graphene during the faradaic redox reaction.

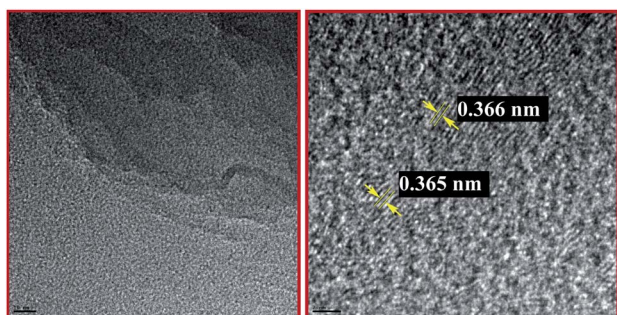


Fig. 2 Representative HRTEM images of graphene oxide. Scale bars are 10 nm and 2 nm in the left and right panel, respectively.

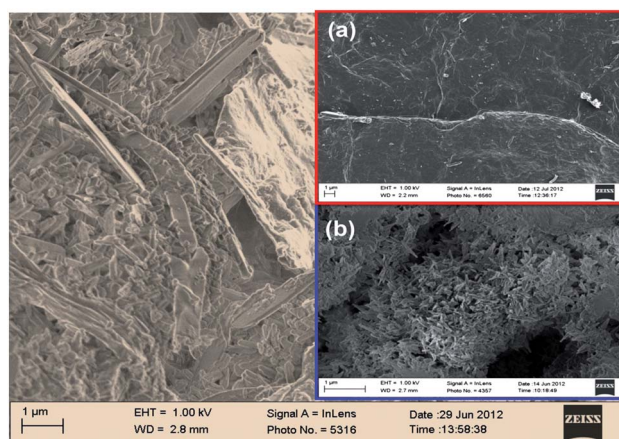


Fig. 3 FESEM image of the GO/CoTPyzPz hybrid. Insets represent (a) GO and (b) CoTPyzPz: scale bars = 1  $\mu$ m.

The GO/CoTPyzPz hybrid produced a thick, small-sized globular structure (0.1–0.3  $\mu$ m), presumably due to the face-to-face interaction between the molecules as seen from AFM measurements in Fig. SI 1.† From the Raman spectra (Fig. SI 2†), there is an increase in the D to G band intensity ratio,  $I_D/I_G$ , from 0.87 to 0.91 upon integration of GO with CoTPyzPz, reflecting a disorder in the carbon structure. Both the Raman and IR (Fig. SI 3†) spectra gave the characteristic peaks of the metallopyrazinoporphyrazines.

#### Electrochemical studies

Fig. 5 shows typical conventional three-electrode cyclic voltammetric evolutions of the GO, CoTPyzPz, and GO-CoTPyzPz in 1 M  $\text{Na}_2\text{SO}_4$ . The current/capacitance responses of the individual molecules are much lower than their composite (GO/CoTPyzPz). The higher electrochemical activity of the composite may be related to redox-activities (pseudo-capacitance) of the oxygen-groups of the GO, the high nitrogen content of the porphyrazine rings, and the central metal of the porphyrazine (Co(II)/Co(III)) as manifested by the pair of voltammetric peaks. It is known that the pyrrol and pyridinic nitrogens enhance supercapacitance.<sup>15</sup>

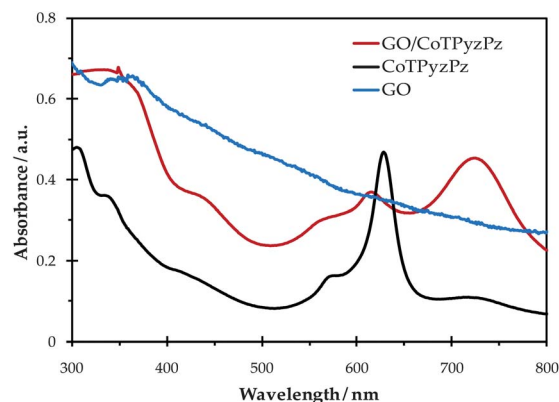


Fig. 4 UV-vis spectra of GO, CoTPyzPz, and GO/CoTPyzPz in DMF.

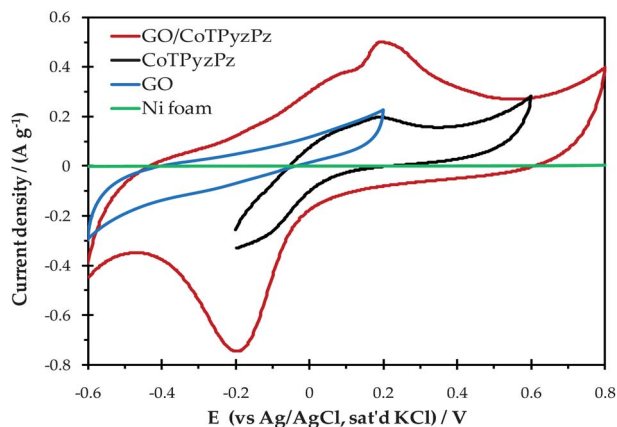


Fig. 5 Cyclic voltammetric evolutions of GO, CoTPyzPz, and GO-CoTPyzPz in 1 M Na<sub>2</sub>SO<sub>4</sub>.

The pyrrol or pyrrol-like nitrogens (-NH) improve charge mobility in a carbon matrix by their ability to introduce electron-donor characteristics and enhancing the carbon catalytic activity in electron-transfer reactions, while the pyridinic nitrogens (=N) can provide a lone pair for conjugation with the  $\pi$ -conjugated rings.

The supercapacitive properties were evidenced by the galvanostatic charge-discharge experiments at different current densities, as exemplified in Fig. 6. The specific capacitance ( $C_{sp}$ ), maximum specific power density ( $P_{max}$ ) and specific energy density ( $E$ ) were determined from the discharge process using the established equations (eqn (1)–(4)) for a 2-electrode (full cell) device:<sup>23</sup>

$$C(F) = \frac{i}{\Delta V/\Delta t} \quad (1)$$

$$C_{sp}(F \text{ g}^{-1}) = \frac{4C}{m} \quad (2)$$

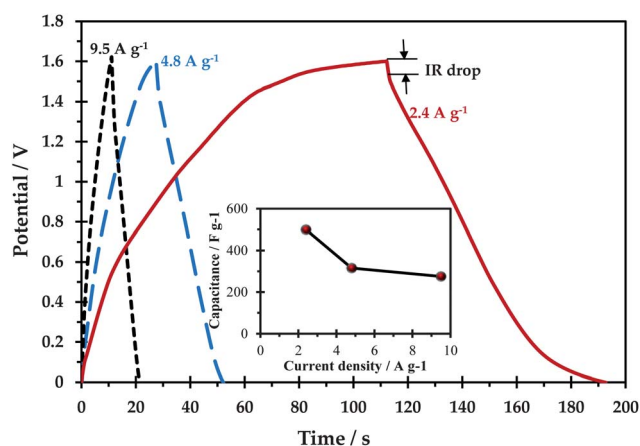


Fig. 6 Galvanostatic charge-discharge curves of GO/CoTPyzPz in 1 M Na<sub>2</sub>SO<sub>4</sub> at different current densities and the inset showing the capacitance as a function of current density.

$$P_{max}(\text{W kg}^{-1}) = \frac{V^2}{4R_{ir}m} \quad (3)$$

$$E(\text{W h kg}^{-1}) = \frac{CV^2}{2m} \quad (4)$$

where  $i$  is the applied current,  $\Delta V/\Delta t$  is the slope of the discharge curve after the initial  $iR$  drop,  $m$  is the mass of the active materials of each electrode (anode and cathode),  $V$  is the applied voltage,  $C$  is the measured total capacitance, and  $R_{ir}$  is the internal resistance determined from the voltage drop at the beginning of each discharge:

$$R_{ir}(\Omega) = \frac{\Delta V_{iR}}{2i} \quad (5)$$

where  $\Delta V_{iR}$  is the voltage drop between the first two points from its top cut-off.

Note from the inset of Fig. 6 that the device showed best responses only at high current densities ( $\geq 2 \text{ A g}^{-1}$ ). From the Ragone plot at different current densities (Fig. 7), the energy density decreased from  $44 \text{ W h kg}^{-1}$  at a power density of  $31 \text{ kW kg}^{-1}$  (at  $2.4 \text{ A g}^{-1}$ ) to  $24 \text{ W h kg}^{-1}$  at a power density of  $41 \text{ kW kg}^{-1}$  (at  $9.5 \text{ A g}^{-1}$ ), which is higher than the power target of the Partnership for a New Generation of Vehicles (PNGV,  $15 \text{ kW kg}^{-1}$ ),<sup>24</sup> thus supporting the applicability of GO/CoTPyzPz//CB-GO based supercapacitors as effective power supply components in hybrid vehicle systems.

In fact, the energy density of the GO/CoTPyzPz//GOCB based AEC falls within the range usually observed for the nickel metal hydride (NiMH) battery (*i.e.*  $30\text{--}100 \text{ W h kg}^{-1}$ ); more importantly, has a much better power performance than the NiMH battery ( $0.25\text{--}1 \text{ kW kg}^{-1}$ ) widely used today in hybrid vehicles such as Toyota Prius and Honda Insight.<sup>25</sup>

In addition, the asymmetric GO/CoTPyzPz//CB-GO supercapacitor exhibits a maximum energy density of  $44 \text{ W h kg}^{-1}$  at a power density of  $31 \text{ kW kg}^{-1}$ , and still maintains  $24 \text{ W h kg}^{-1}$  at a power of  $41 \text{ kW kg}^{-1}$ , comparable or even higher than the best-performing asymmetric electrochemical capacitors studied in the same neutral aqueous electrolyte conditions ( $1 \text{ M Na}_2\text{SO}_4$ )

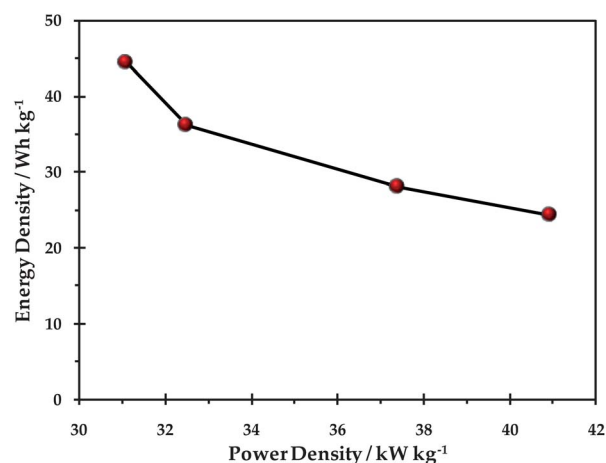


Fig. 7 Ragone plot (specific energy versus specific power density) of the GO/CoTPyzPz//GOCB based AEC.

such as the MnO<sub>2</sub> nanowire–graphene composite (30 W h kg<sup>-1</sup> at 0.1 kW kg<sup>-1</sup>)<sup>26</sup> and MnO<sub>2</sub>–graphene composite (51 W h kg<sup>-1</sup> at 0.198 kW kg<sup>-1</sup>).<sup>27</sup>

To explore the cycling stability, the GO/CoTPyzPz//GOCB based AEC was subjected to continuous electrochemical cycling up to 1000 cycles at a high current density of 2.4 A g<sup>-1</sup> (Fig. 8). The AEC maintained a stability at ~410 F g<sup>-1</sup> until about the 400<sup>th</sup> cycle from where it decreased. Interestingly, the AEC maintained a specific capacitance of ca. 240 F g<sup>-1</sup> at the 1000<sup>th</sup> cycle. This loss in capacitance may be related to the loss of adhesion of some active material with the current collector during the continuous cycling process.

The energy deliverable efficiency ( $\eta$ %) was obtained from eqn (6)

$$\eta(\%) = \frac{t_d}{t_c} \times 100 \quad (6)$$

where  $t_d$  and  $t_c$  are the total amount of discharge and charging times, respectively. The energy deliverable efficiency of the GO/CoTPyzPz was >99%, meaning that the device can be charged and discharged continuously at a very high current density without a detectable loss in coulombic efficiency.

From the EIS data shown in Fig. 9, it is very interesting to observe that the equivalent series resistance (ESR) before and after 1000 cycles remained essentially the same (from 1.46 to 1.63  $\Omega$ ) indicating that the new AEC hybrid device maintains its electronic conductivity (*i.e.*, little or no poisoning of the electrode–electrolyte interface) even after several electrochemical cyclings. The response time ( $t_R$ ), determined from the “knee” or “onset” frequency ( $f_o$ ) is about 16 ms, suggesting that most of its stored energy is still accessible at frequencies as high as 63 Hz. Most commercially available supercapacitors, including those specifically designed for higher power applications, operate at frequencies less than 1 Hz.<sup>28</sup> From the Bode plots, the phase angle decreased from 76 to 62 degrees, indicating further transition to more pseudocapacitive properties. There is also a slight change in the polarisation resistance after 1000 cycles (from 0.34 to 0.50  $\Omega$ ), which may be due to loss of adhesion of some active material with the current collector during cycling.

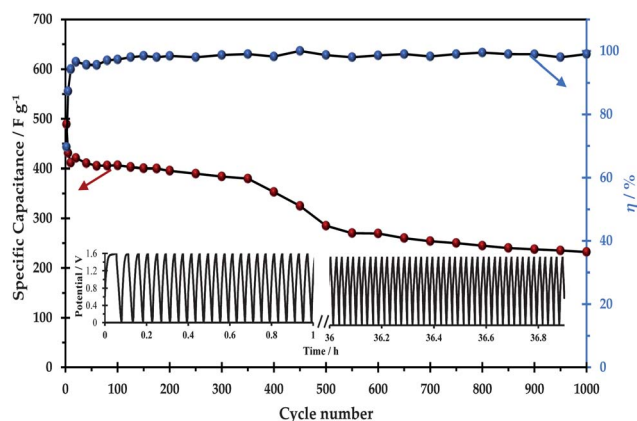


Fig. 8 Cycling stability and efficiency plots of the GO/CoTPyzPz//GOCB based AEC in 1 M Na<sub>2</sub>SO<sub>4</sub> and the inset showing the charge discharge curves.

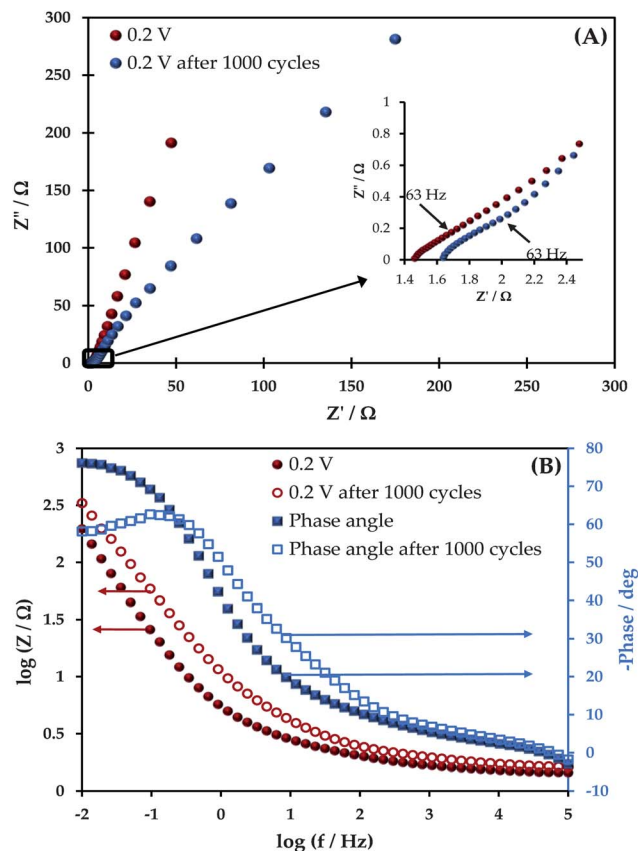


Fig. 9 (A) The Nyquist plots with an inset showing the “knee” frequencies before and after the 1000<sup>th</sup> cycle, and (B) the corresponding Bode plots of the Nyquist plots.

## 4 Conclusions

The electrochemical capacitive properties of a novel aqueous asymmetric electrochemical capacitor based on a GO/CoTPyzPz nanocomposite have been reported. The specific capacitance, high energy density and power density (~500 F g<sup>-1</sup>, 44 W h kg<sup>-1</sup>, 31 kW kg<sup>-1</sup>) coupled with long cycle life, short response time, and low ESR clearly indicate that this asymmetric supercapacitor is potentially useful in developing low-cost and ‘green’ energy storage devices with high capacitance, energy and power densities.

## Acknowledgements

This work was supported by the University of Pretoria, CSIR and NRF Nanotechnology flagship programme (K.I.O), and the US National Science Foundation (CHE-1012258 and DMR-0804049, S.W.C.).

## Notes and references

- M. J. Danzig, C. Y. Liang and E. J. Passaglia, *J. Am. Chem. Soc.*, 1963, **85**, 668.
- D. Dini, M. Hanack, H.-J. Egelhaaf, J. C. Sancho-Garcia and J. Cornil, *J. Phys. Chem. B*, 2005, **109**, 5425.

- 3 D. Dini, M. Hanack and M. Meneghetti, *J. Phys. Chem. B*, 2005, **109**, 12691.
- 4 G. De Mori, Z. Fu, E. Viola, X. Cai, C. Ercolani, M. P. Donzello and K. M. Kadish, *Inorg. Chem.*, 2011, **50**, 8225.
- 5 N. Kobayashi, K. Adachi and T. Osa, *Anal. Sci.*, 1990, **6**, 449.
- 6 A. T. Chidembo, K. I. Ozoemena, B. O. Agboola, V. Gupta, G. G. Wildgoose and R. G. Compton, *Energy Environ. Sci.*, 2010, **3**, 228.
- 7 J. Oni and K. I. Ozoemena, *J. Porphyrins Phthalocyanines*, 2012, **16**, 754–760.
- 8 J. Mu, C. Shao, Z. Guo, M. Zhang, Z. Zhang, P. Zhang, B. Chen and Y. Liu, *Nanoscale*, 2011, **3**, 5126.
- 9 R. Kotz and M. Carlen, *Electrochim. Acta*, 2000, **45**, 2483.
- 10 Y. Wang, Z. Shi, Y. Huang, Y. Ma, C. Wang, M. Chen and Y. Chen, *J. Phys. Chem. C*, 2009, **113**, 13103.
- 11 B. Xu, S. Yue, Z. Sui, X. Zhang, S. Hou, G. Cao and Y. Yang, *Energy Environ. Sci.*, 2011, **4**, 2826.
- 12 E. Raymundo-Piñero, M. Cadek and F. Béguin, *Adv. Funct. Mater.*, 2009, **19**, 1032.
- 13 C. T. Hsieh and H. Teng, *Carbon*, 2002, **40**, 667.
- 14 Q. Bao, S. Bao, C. Li, X. Qi, C. Pan, J. Zang, Z. Lu, Y. Li, D. Y. Tang, S. Zhang and K. Lian, *J. Phys. Chem. C*, 2008, **112**, 3612.
- 15 D. Hulicova-Jurcakova, M. Kodama, S. Shiraishi, H. Hatori, Z. Zhu and G. Lu, *Adv. Funct. Mater.*, 2009, **19**, 1800–1809.
- 16 F. C. Su, K. Poh, J. S. Chen, G. Xu, D. Wang, Q. Li, J. Lin and X. W. Lou, *Energy Environ. Sci.*, 2011, **4**, 717.
- 17 J. W. Long, D. Bélanger, T. Brousse, W. Sugimoto, M. B. Sassin and O. Crosnier, *MRS Bull.*, 2011, **36**, 513.
- 18 Q. Cheng, J. Tang, J. Ma, H. Zhang, N. Shinya and L.-C. Qin, *Phys. Chem. Chem. Phys.*, 2011, **13**, 17615.
- 19 W. S. Hummers and R. E. Offeman, *J. Am. Chem. Soc.*, 1958, **80**, 1339.
- 20 H. P. Boehm, *Carbon surface chemistry in Graphite and Precursors*, Gordon and Breach Science Publishers, Pessac, France, 1st edn, 2001.
- 21 K. I. Ozoemena and T. Nyokong, *J. Chem. Soc., Dalton Trans.*, 2002, 1806.
- 22 K. Nakai, K. Ishii and N. Kobayashi, *J. Phys. Chem. B*, 2003, **107**, 9749.
- 23 P. Chen, H. Chen, J. Qiu and C. Zhou, *Nano Res.*, 2010, **3**, 594.
- 24 D. W. Wang, F. Li, M. Liu, G. Q. Lu and H.-M. Cheng, *Angew. Chem., Int. Ed.*, 2008, **47**, 373.
- 25 Q. Cheng, J. Tang, J. Ma, H. Zhang, N. Shinya and L.-C. Qin, *Phys. Chem. Chem. Phys.*, 2011, **13**, 17615.
- 26 Z.-S. Wu, W. Ren, D.-W. Wang, F. Li, B. Liu and H.-M. Cheng, *ACS Nano*, 2010, **4**, 5835.
- 27 Z. Fan, J. Yan, T. Wei, L. Zhi, G. Ning, T. Li and F. Wei, *Adv. Funct. Mater.*, 2011, **21**, 2366.
- 28 J. R. Miller, *Extended Abstracts of Electrochemical Society*, 1995, **66**, 246.